Combust. Theory Modelling 2 (1998) 405–422. Printed in the UK PII: S1364-7830(98)88444-1

A radiative transport model for large-eddy fire simulations

H R Baum† and W E Mell

National Institute of Standards and Technology, Gaithersburg, MD 20899, USA

Received 15 October 1997, in final form 15 July 1998

Abstract. Three-dimensional simulations of fires cannot be performed on present-day computers without devising simplifications to the governing equations. One such method is the large-eddy simulation (LES) approach for fires developed at NIST. This method results in computationally efficient fire simulations in which the buoyancy-generated motion of hot gases and smoke is driven by Lagrangian particles that carry the heat released by combustion. Complex geometries are represented by blocking cells interior to a rectangular domain. A P1 approximation to the radiation transport equation was developed to be consistent with the exact transport equation for scenarios based upon this model. An isolated fire plume above a semi-infinite solid with a constant absorption coefficient in each half-space was studied as an example. A direct elliptic solver required only a fraction of the total LES computational cost. Radiative fluxes and intensities from the numerical and exact solutions to the P1 approximation were in excellent agreement.

1. Introduction

Thermal radiation and buoyant convection are the dominant modes of heat transfer in large fires. Even in small pool fires (diameter of 0.1–0.3 m) radiative feedback to the fuel surface is significant [1]. The purpose of this paper is to describe a model of radiative transport in gases that is suitable for use with a large-eddy simulation (LES) approach for fire dynamics developed at NIST (National Institute of Standards and Technology) [2, 3]. This LES model of convective transport and combustion heat release was developed by distinguishing between physical processes that can be computed explicitly and those that operate at length and time scales too small to be resolved (i.e. subgrid). A consequence of this approach is that most computational resources can be devoted to the large-scale transport of hot gases and smoke induced by the buoyantly induced flow. This is highly desirable in fire safety simulations of the kind for which the LES approach is designed (e.g. warehouse or building fires). The same strategy will be attempted here for the thermal radiation generated by the fire.

For the present purposes it is sufficient to understand that the fluid mechanics is calculated on an Eulerian finite-difference grid in rectangular coordinates. The velocity and temperature fields calculated in this way are assumed to be large-scale phenomena resolvable on the grid. Complex geometries are incorporated by blocking computational cells corresponding to internal boundaries in a rectangular computational domain. The combustion phenomena that buoyantly drive the flow are assumed to be subgrid scale, whose consequences can be represented by Lagrangian 'thermal elements'. These elements

† Author to whom correspondence should be addressed.

1364-7830/98/040405+18$19.50

release sensible energy into the gas as they are convected with the large scale fluid motion. A description and justification of this procedure can be found in [3, 4].

In the analysis of radiative transport, it will be assumed that part of the energy released as a result of the combustion processes is emitted as thermal radiation. This implies that the emission processes are also subgrid scale, and cannot be calculated on a macroscopic grid equivalent to that used for the fluid mechanics. The absorption and transport of radiation, however, are both assumed to take place on scales set by the large scale fluid motion and the enclosure or scenario geometry, if any. Thus, these phenomena are resolved explicitly in the model and computations described below. This implies that the radiation fields are far from equilibrium in the fire scenarios of interest here. In effect, the radiation is treated in a manner analogous to the combustion phenomena that generate it. The crucial point in the analysis is that the *energy release*, not the temperatures in the subgrid scale phenomena, must be captured. The subgrid combustion physics also controls the soot generation. This can be accounted for by defining the local soot mass distribution as a property associated with the 'thermal elements'. This information could be converted into grid-based information as needed, in exactly the same way as the combustion heat release is for the computation of the convective transport.

The inability to resolve small-scale combustion and radiative emission processes in any detail is not only due to limitations on computer resources. Most of the 'fuels' consumed in fires were never intended as such. Hence, thermophysical and chemical properties of the kind needed to analyse the combustion of the contents of a room or warehouse, for example, are simply unavailable. Thus, it makes no sense to attempt to resolve either the spectral or angular dependence of the thermal radiation in any detail. Instead, a version of the 'P1' approximation [11] is adapted to the typical fire scenario and a grey-gas model is employed to describe the absorption.

With the adoption of the P1 approximation, complex geometries can be treated approximately by regarding physical barriers to the flow as highly absorbing media. While this may appear at first sight to be a very crude approximation to the interaction of radiation with a typical surface, it has some important virtues as well. First, as shown below, it implies boundary conditions very similar to those typically used with the P1 model. Second, the physical assumptions made are quite plausible; especially when one considers the soot-coated surfaces present in most fires. Finally, since the radiative transport problem then becomes the solution to a self-adjoint partial differential equation in a rectangular domain, efficient solution techniques can be employed. This is a crucial point since typical applications require million-cell grids with the solution available on each of thousands of time steps.

A number of approximate techniques are used for the treatment of radiative transport in other present-day CFD-based fire simulations. These include the six-flux model [5] for two-dimensional and the discrete transfer method [6] for three-dimensional (but with assumed centreline symmetry) simulations of grey-gas enclosure fires. For their two-dimensional flame spread simulations Yan and Homstedt [7] approximate the spectral dependence by combining a narrow-band model with the discrete transfer method. Another method, used by Bressloff *et al* [8] in their axisymmetric simulation of a turbulent jet diffusion flame, is to incorporate a weighted sum of grey-gases solution into the discrete transfer method. The different discrete transfer approaches vary mostly according to the degree to which the spectral dependence of the radiation is included. Computational cost limits the complexity of the radiation model in fire simulations. Bedir *et al* [9] compared approximate solution techniques for a one-dimensional diffusion flame. In order of decreasing computational cost they considered narrow-band, wide-band, spectral-line-weighted summation of grey gases

(both 30 and 3 grey gases), and grey-gas approximations. CPU times, weighted by the grey-gas computation, were found to be 630, 150, 110 and 9, respectively.

These earlier studies clearly demonstrate that even the crudest approach to including spectral dependence was nearly an order of magnitude more expensive than the grey-gas model. Any realistic analysis of the spectral dependence imposes a two order of magnitude penalty in computational time. Those calculations that included spectral dependence contained at most 2000 grid cells, two space dimensions, and PMMA as the solid fuel. All three-dimensional calculations reported to date have used a grey-gas model.

As mentioned above, the LES approach was designed for three-dimensional simulations of fires with an emphasis on the spatial resolution of the buoyant transport of smoke and hot gases. This emphasis on spatial resolution is, in fact, the defining feature of the LES fire simulations relative to the other CFD-based approaches referenced above. For example, the highest resolved case reported by Lewis *et al* [6] (three-dimensional enclosure fire with constant absorption coefficient) used 70 000 grid points. Fire simulations with 10^6 grid points are routinely performed with the LES approach. It is crucial therefore, to use a radiation model which does not require a sacrifice in spatial resolution. Thus, the grey-gas approximation is consistent with the information available for fire scenarios, and is in line with other state-of-the-art approaches for *three-dimensional* fire simulation.

The remainder of the paper is organized as follows: the next section introduces the P1 approximation in the form needed for LES fire simulations. Boundary conditions are developed using continuity of integrated intensity and radiant energy flux, and compared with more conventional approaches. Section 3 compares the results of the P1 model with the exact transport equation for a collection of highly localized energy sources used to characterize fires. Section 4 presents the analytical solution to the P1 model for a collection of sources adjacent to a semi-infinite boundary. This illustrates how solid boundaries are represented, and serves as a testbed for the numerical solution presented in section 5. This solution uses the LES code to represent the fire and an FFT-based direct solver for the P1 model. The boundary is not introduced explicitly; only a rapid increase in the absorption coefficient is needed to obtain results very close to the analytical solutions. Some general remarks close the paper.

2. The radiative transport model

The starting point for the analysis is the radiative transport equation for a non-scattering grey gas [10]

$$\Omega \cdot \nabla I(r,\ \Omega) = \kappa(r)\left(\frac{\sigma T(r)^4}{\pi} - I(r,\ \Omega)\right). \tag{1}$$

Here, $I(r,\ \Omega)$ is the radiant intensity, defined so that $I(r,\ \Omega)\,\mathrm{d}\Omega$ is the radiant energy at a point r passing through a unit area per unit time through the element of solid angle $\mathrm{d}\Omega$ centred about the direction Ω. The grey-gas absorption coefficient is $\kappa(r)$, and the local temperature is $T(r)$. The quantity σ is the Stefan–Boltzmann constant. Both the spectral dependence of the radiation and the scattering have been ignored because, in addition to computational expense, in the emitting regions where they are likely to be important, the relevant processes cannot be spatially resolved; while in the spatially extended soot clouds, absorption is the most important mechanism.

The radiant heat flux vector $q(r)$ can be defined in terms of the radiant intensity as follows:

$$q(r) = \int \Omega I(r,\ \Omega)\, d\Omega. \tag{2}$$

Here, the integral is taken over all 4π sr since the radiation at a point can be coming from any direction. Similarly, the integrated radiant intensity $U(r)$ is defined as

$$U(r) = \int I(r,\ \Omega)\, d\Omega. \tag{3}$$

Note that $U(r)/c$ is the radiant energy density and c is the speed of light. Using this definition and integrating equation (1) over all Ω yields the conservation of radiant energy equation

$$\nabla \cdot q(r) = \kappa(r)\left[4\sigma T(r)^4 - U(r)\right]. \tag{4}$$

This equation is simply a statement that the net radiant energy flux out of any region occupied by the gas is the difference between that emitted and that absorbed in the volume under consideration. This energy exchange between the radiation field and the gas is what couples the convective transport and radiative transport in the bulk of the gas. The coupling at gas–surface interfaces will be considered briefly below.

The dependence of each physical quantity on r and Ω is shown explicitly since this constitutes the principal mathematical and computational difficulty associated with radiative transport. Since the radiant intensity at each instant of time depends on five independent variables (Ω is a unit vector), the direct solution of equation (1) is prohibitively difficult. Some drastic approximation is needed; especially when the high-resolution grids needed for convective transport are considered. There are two basic choices available. First, the spatial resolution can be reduced to the point where the number of grid points in each direction is comparable to the number of direction cosines retained for computational purposes. Alternatively, the high spatial resolution could be retained but an explicit simplifying form can be chosen for the dependence of the radiant intensity on Ω. The latter choice is made here.

There are two main reasons for this choice. First, since high spatial resolution is needed for the description of convective transport, it follows that the sources and sinks of radiation that appear in the radiant energy equation (4) must have a considerably fine structure. Cutting back on the spatial resolution to accommodate a high angular resolution might well undermine the description of convective transport. Second, the 'diffusion approximation', in the sense of [10], gives results that are accurate enough for the present application, especially when the approximations already made in the radiative transport equation (1) are taken into account.

To proceed, following [10], note that equation (4) gives one relationship between U and q. It arises from the zeroth moment of equation (1) with respect to Ω. If a suitable functional form for I as a function of Ω that preserves the next (vector) moment of this equation can be found involving only U and q, then a closed system of equations will result. The existence of such a form is well known; in the present notation it can be written as

$$I(r,\ \Omega) = \frac{1}{4\pi}\,(U(r) + 3q \cdot \Omega). \tag{5}$$

This choice preserves the first four scalar moments of the radiative transport equation, and closes the system with the relation

$$\nabla U(r) = -3\kappa(r)\, q(r). \tag{6}$$

With this relation for the radiant heat flux vector and equation (4), the conservation equation for the integrated intensity is

$$\nabla \cdot \frac{1}{\kappa(r)} \nabla U(r) - 3\kappa(r)\, U(r) = -3\kappa(r)\, 4\sigma T^4(r). \tag{7}$$

Equation (7) is known as the P1 approximation to the radiation transfer equation [11].

2.1. Boundary conditions

The role of condensed phase boundaries using the P1 model will be considered next. The first step is to derive a suitable set of conditions for the gas phase radiation. There are two possible approaches worth considering. To discuss these in concrete terms, consider the scenario illustrated in figure 1. The gaseous medium occupies the upper half-space $y \geqslant 0$. The lower half-space contains the condensed phase material at temperature T_s with absorption coefficient κ_s. Clearly the scale is sufficiently small in macroscopic terms for the boundary to be regarded as planar and the temperature locally uniform.

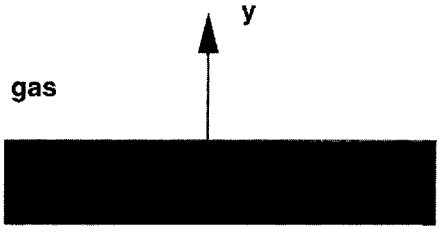

Figure 1. Schematic of the interface between gas and condensed phase, the temperature of the solid T_s is uniform in the region shown.

In the condensed phase the integrated intensity U_s satisfies the equation

$$-\frac{1}{3\kappa_s^2}\frac{d^2U_s}{dy^2} + U_s = 4\sigma T_s^4. \tag{8}$$

The solutions bounded as $y \to -\infty$ for U_s and the condensed phase radiant heat flux vector q_s take the form

$$U_s = 4\sigma T_s^4 - a\exp(\sqrt{3}\kappa_s y) \tag{9}$$

$$q_s = \frac{a}{\sqrt{3}}\exp(\sqrt{3}\kappa_s y). \tag{10}$$

Eliminating the constant a between equations (9) and (10) yields the following relation:

$$U_s + \sqrt{3}q_s = 4\sigma T_s^4. \tag{11}$$

Following Zeldovich [10], we require that the integrated intensity and the heat flux vector are continuous at the interface between the gas and condensed phase. The quantities U_s and q_s can then be replaced by their gas phase equivalents. Thus, if n denotes a unit

normal to the surface pointing *into* the gas, the boundary condition can be written in the more general form:

$$U(\boldsymbol{r}) + \sqrt{3}\,\boldsymbol{n} \cdot \boldsymbol{q}(\boldsymbol{r}) = 4\sigma T_s^4(\boldsymbol{r}). \tag{12}$$

This result should be compared with an alternative boundary condition proposed by Vincenti and Kruger [13]. They assume that the functional form given by equation (5) is valid for $\boldsymbol{\Omega} \cdot \boldsymbol{n} < 0$, and that for $\boldsymbol{\Omega} \cdot \boldsymbol{n} > 0$ the wall emits black body radiation at the surface temperature T_s. The result is the following boundary condition:

$$U(\boldsymbol{r}) + 2\,\boldsymbol{n} \cdot \boldsymbol{q}(\boldsymbol{r}) = 4\sigma T_s^4(\boldsymbol{r}). \tag{13}$$

The only difference is that the factor $\sqrt{3}$ in the coefficient of the heat flux contribution to the boundary condition is replaced by 2. There are several reasons to prefer equation (12) to work with. First, it is just as valid on fundamental physical grounds as equation (13). Second, it permits absorption in depth in the condensed phase to be considered, a phenomenon which is important for some materials (see Pagni [14]). Finally, it permits the introduction of solid obstacles in the interior of the computational domain. These can be analysed by considering them as highly absorbing materials, so that the radiation incident on one side does not penetrate to the other. Even if the penetration depth is grossly exaggerated in the computation, the results in the gas phase will be largely unaffected. Note that reflection from the boundary is not considered the formulation of the boundary conditions. While the P1 approximation does not preclude the use of reflecting boundary conditions (as in, for example, a zero flux condition for a perfectly reflecting boundary) this issue was not pursued in the analysis to date.

3. Comparison with exact transport equation

We now wish to compare the way in which the P1 model equations (4) and (6) predict the transport of radiation with corresponding results from the exact transport equation (1) in simplified situations that are relevant to the typical fire scenario. The simplest of these is the case of an unbounded domain with a uniform absorption coefficient. The gas is assumed to depart from a uniform ambient temperature T_∞ in a large number of finite regions of arbitrary size or shape. This scenario is an idealized representation of the interior of a heavily soot laden smoke plume. Ultimately, the assumption that the background temperature and absorption coefficient are constant will be dropped. However, the idea that the emitting regions are compact and scattered throughout the fire plume is entirely consistent with the present authors representation of combustion energy release in large-eddy fire simulations. The scenario appropriate to the solution is sketched in figure 2.

Since the spatial distribution of radiant energy is determined by the Green function in the absence of boundaries, the most logical way to assess the accuracy of the P1 model is to compare the Green function associated with equation (7) with the corresponding result from equation (1). Since the transport equation is linear, attention is focused on a single region of finite extent. The radiant intensity $I(\boldsymbol{r}, \boldsymbol{\Omega})$ is written in the form:

$$I(\boldsymbol{r}, \boldsymbol{\Omega}) = \frac{\sigma T_\infty^4}{\pi} + \int \frac{\kappa\sigma}{\pi} \left(T(\boldsymbol{r}_0)^4 - T_\infty^4\right) G_e(\boldsymbol{r} - \boldsymbol{r}_0, \boldsymbol{\Omega})\, \mathrm{d}\boldsymbol{r}_0 \tag{14}$$

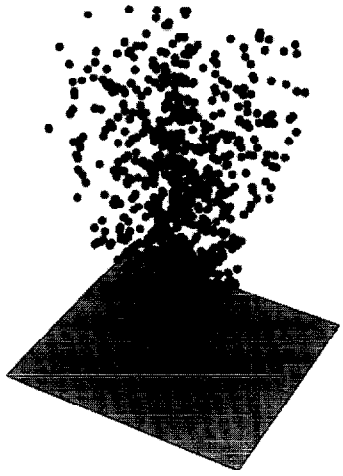

Figure 2. Schematic showing discrete emitters in fire plume smoke cloud.
(This figure can be viewed in colour in the electronic version of the article; see http://www.iop.org)

where T_∞ and $I_\infty = \sigma T_\infty^4/\pi$ are the far field temperature and intensity, respectively. The exact Green function $G_e(r - r_0, \Omega)$ satisfies the equation

$$\Omega \cdot \nabla G_e + \kappa G_e = \delta(r - r_0). \tag{15}$$

The solution can be readily obtained using Fourier transform techniques. Let $x = \kappa(r - r_0)$ and define the Fourier transform $G^*(k, \Omega)$ as follows:

$$G^*(k, \Omega) = \int \mathrm{d}x \, \exp(-\mathrm{i}k \cdot x) \, G_e(x, \Omega). \tag{16}$$

Taking the transform of equation (15) yields the solution for G^* in the form:

$$G^* = \kappa^2 \left(\frac{1}{1 + \mathrm{i}k \cdot \Omega} \right). \tag{17}$$

Now the quantity of physical interest is the radiant heat flux vector associated with the Green function. Defining $q^*(k)$ as its Fourier transform, using equation (2) we have

$$q^*(k) = \int G^* \, \Omega \, \mathrm{d}\Omega. \tag{18}$$

Since G^* depends only upon $k \cdot \Omega$, the integration over Ω and the absence of any other vectors leads to the requirement that $q^*(k)$ has the form

$$q^* = -\mathrm{i}k\phi^*(k). \tag{19}$$

Taking the scalar product of equation (19) with k and using equation (17) yields the following expression for $\phi^*(k)$:

$$\phi^* = -\frac{2\pi\kappa^2}{k^2} \left(\frac{1}{\mathrm{i}k} \log \left[\frac{1 + \mathrm{i}k}{1 - \mathrm{i}k} \right] - 2 \right). \tag{20}$$

The Fourier transform can be inverted by noting that since ϕ^* depends only on k. The result is

$$\phi(x) = \frac{\kappa^2}{x} E_2(x). \tag{21}$$

Here, $E_2(x)$ denotes the exponential integral function. Finally, taking the gradient of ϕ with respect to $\boldsymbol{x}$, the desired result is obtained:

$$q_G(\boldsymbol{x}) = \kappa^2 \frac{\boldsymbol{x}}{x}\left[\frac{\exp(-x)}{x^2}\right]. \tag{22}$$

In order to compare the exact and diffusion model results, equation (14) is integrated over all Ω. Then using equation (22) and assuming that the point $\boldsymbol{r}$ is outside the emitting region:

$$q_e = Q\frac{\boldsymbol{R}}{R}\frac{\exp(-\kappa R)}{4\pi R^2}. \tag{23}$$

Here, the vector $\boldsymbol{R}$ is the line from the centroid of the emitting region to the point $\boldsymbol{r}$, while Q is the total radiative power emitted from the region:

$$Q = \int 4\kappa\sigma\left(T(\boldsymbol{r})^4 - T_\infty^4\right) \mathrm{d}\boldsymbol{r}. \tag{24}$$

We now wish to investigate the way in which the P1 model equations (4) and (6) predict the transport of radiation in the same scenario. Again, the gas is assumed to depart from a uniform ambient temperature T_∞ in one or more finite regions of arbitrary size or shape. Far from any of the regions of elevated temperature, $U \to U_\infty$, where $U_\infty = 4\sigma T_\infty^4$. Thus, for this problem the model equations can be written as

$$U = U_\infty + V(\boldsymbol{r}), \tag{25}$$

$$\nabla^2 V - 3\kappa^2 V = -3\kappa^2 4\sigma\left(T^4 - T_\infty^4\right). \tag{26}$$

The only boundary condition is that $V \to 0$ at infinity.

The solution can be readily obtained in terms of a Green function $G(\boldsymbol{r}-\boldsymbol{r}_0)$ that satisfies the equation

$$\nabla^2 G - 3\kappa^2 G = \delta(\boldsymbol{r} - \boldsymbol{r}_0). \tag{27}$$

Since neither equation (27) nor the boundary conditions exhibit any preferred direction, the solution for G must be spherically symmetric in $\boldsymbol{r} - \boldsymbol{r}_0$. It is readily found to be

$$G(\boldsymbol{r} - \boldsymbol{r}_0) = -\frac{1}{4\pi|\boldsymbol{r} - \boldsymbol{r}_0|}\exp\left(-\sqrt{3}\kappa|\boldsymbol{r} - \boldsymbol{r}_0|\right). \tag{28}$$

Using this result, the solution for the integrated intensity can be written in the form:

$$U = U_\infty + \int 3\kappa^2 4\sigma\left(T(\boldsymbol{r}_0)^4 - T_\infty^4\right) G(\boldsymbol{r} - \boldsymbol{r}_0)\,\mathrm{d}\boldsymbol{r}_0. \tag{29}$$

Here, the integral is over all space. Now if the temperature rise is restricted to N disjoint regions of finite extent, then equation (29) can be used to derive the following expression for the radiation heat flux:

$$q(\boldsymbol{r}) = -\sum_{n=1}^{N}\int 4\kappa\sigma\left(T(\boldsymbol{r}_n)^4 - T_\infty^4\right)\nabla_r\left(G(\boldsymbol{r} - \boldsymbol{r}_n)\right)\mathrm{d}\boldsymbol{r}_n. \tag{30}$$

There are several points relevant to the fire scenario contained in the solution. First, the emission and absorption of radiation are treated very differently in the analysis. The emission is a 'known' source term from the perspective of radiative transport. The absorption, however, determines the structure of the transport equation. This can be seen by noting that the solution is linear in $\kappa\left(T^4 - T_\infty^4\right)$, but the absorption length scale $(\sqrt{3}\kappa)^{-1}$ is built into the Green function in a non-trivial way. This permits the absorption and emission to occur on very different length scales. Indeed, since the emission is proportional to a high power

of the temperature, it mostly occurs in or near the highly localized flame sheets where the combustion takes place. Both gaseous and particulate combustion products contribute to the emission of radiation [12]. The absorption of radiation by soot, on the other hand, is relatively insensitive to temperature. Thus, in a heavily soot-laden plume, the entire cloud of smoke can be an efficient absorber of radiation.

The mathematical and computational consequences that result from this separation of scales are critical to this analysis. If we assume the average spacing between each of the emitting regions to be much larger than their spatial extent, then equation (30) can be simplified to the following form:

$$q(r) = -\sum_{n=1}^{N} \frac{R_n}{R_n} \frac{Q_n}{4\pi R_n^2} \exp(-\sqrt{3}\kappa R_n)(1 + \sqrt{3}\kappa R_n). \tag{31}$$

Here, Q_n is the total radiative power emitted from the nth region.

$$Q_n = \int 4\kappa\sigma \left(T(r_n)^4 - T_\infty^4\right) \mathrm{d}r_n. \tag{32}$$

The vector $R_n = r - r_{cn}$ is the line from the centre of energy emission of the nth region r_{cn} to the point in question.

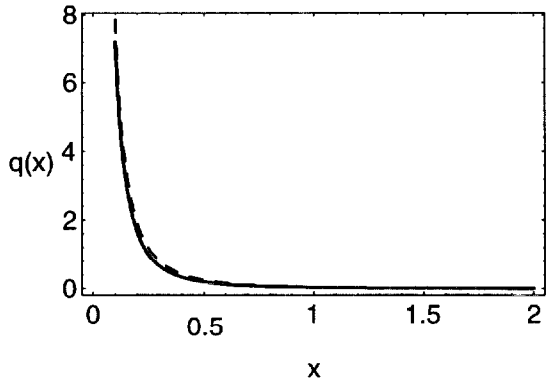

Figure 3. Comparison of radiative flux from point source $q(x)$ as a function of radial optical depth $x = \kappa R$. Full curve, exact solution; broken curve, P1 approximation.

The solutions given by equations (23) and (31) are plotted in figure 3. Note that the two results are very close over the region shown, and agree even more closely as $R \to 0$. Thus, in the bulk of the gas the diffusion model gives excellent results for the scenarios of interest. This is true even if the absorption coefficient vanishes. In fact, in this limit both the exact and approximate radiant heat flux fields become identical, and can be obtained as solutions of the Poisson equation. When κR becomes large, both solutions yield the 'radiation heat conduction' approximation.

4. Semi-infinite domain solution

The concepts introduced in the preceding sections can be assembled to develop a formal solution to the radiative transport problem in a semi-infinite domain. The gas occupies the half-space $y \geqslant 0$. It consists of a background of weakly absorbing gas with $\kappa = \kappa_\infty$ interspersed with a number of compact regions emitting with a total radiative power $\bar{Q}_n$. The

centroid of each region is located at $r = r_n$. The boundary is at temperature $T = T_w(x, 0, z)$. The geometry is the same as that shown in figure 2 with the $y = 0$ plane displayed. There are two objectives of the analysis. First, it shows how a model based on a large number of subgrid scale interacting emitters embedded in an absorbing background can be used to represent the radiation from an isolated fire plume. Then, the same result is obtained numerically to demonstrate that the use of efficient elliptic partial differential equation solvers combined with the notion of a boundary as a strongly absorbing extension of the computational domain allows highly resolved radiation fields to be obtained at relatively modest computational cost. Once again, the starting point is equations (25) and (26). We now make explicit use of the fact that the length scale $(\kappa_\infty)^{-1}$ is assumed to be much larger than any of the emitting regions. Viewed on the large scale, the emitters in the gas phase are a collection of point sources of strength $\tilde{Q}_n$.

To proceed, the solution on the $(\kappa_\infty)^{-1}$ scale satisfies the equation

$$\nabla^2 V - 3\kappa_\infty^2 V = -3\kappa_\infty \sum_{n=1}^{N} \tilde{Q}_n \delta(r - r_n). \tag{33}$$

The solution for V must vanish far from the boundary, while at $y = 0$

$$V - \frac{1}{\sqrt{3}\kappa_\infty} \frac{\partial V}{\partial y} = 4\sigma \left(T_w^4 - T_\infty^4\right). \tag{34}$$

The solution can be expressed in terms of a Green function $G(r, r_0)$ that physically represents the solution corresponding to a point source in the presence of a cold boundary at temperature T_∞. It is defined as the solution to the following equation and surface boundary condition:

$$\nabla^2 G - 3\kappa_\infty^2 G = \delta(r - r_0) \tag{35}$$

$$G - \frac{1}{\sqrt{3}\kappa_\infty} \frac{\partial G}{\partial y} = 0. \tag{36}$$

The solution is obtained by considering the integral $J(r)$ defined over the entire half-space $y \geqslant 0$:

$$J = \int \left\{ G \nabla^2 V - V \nabla^2 G \right\} \mathrm{d}r_0. \tag{37}$$

Applying the divergence theorem and the requirement that G and V vanish at infinity to equation (37) yields a second expression for J:

$$J = \int_{-\infty}^{\infty} \int_{-\infty}^{\infty} \left\{ V(x_0, z_0, 0) \frac{\partial G}{\partial y_0} - G(r, x_0, z_0, 0) \frac{\partial V}{\partial y_0} \right\} \mathrm{d}x_0 \, \mathrm{d}z_0. \tag{38}$$

Next, using equations (33)–(36) in both representations of I and equating them, the following formula for V is obtained:

$$V(r) = -3\kappa_\infty \sum_{n=1}^{N} \tilde{Q}_n G(r, r_n) + V_s(r) \tag{39}$$

$$V_s(r) = -\sqrt{3}\kappa_\infty \int_{-\infty}^{\infty} \int_{-\infty}^{\infty} G(r, r_s) 4\sigma \left(T_w^4 - T_\infty^4\right) \mathrm{d}x_s \, \mathrm{d}z_s. \tag{40}$$

The final step in the solution for V on this scale is the determination of the Green function. This can be accomplished by introducing an auxiliary function $W(\boldsymbol{r}, \boldsymbol{r}_0)$ defined as follows:

$$W(\boldsymbol{r}, \boldsymbol{r}_0) = G - \frac{1}{\sqrt{3}\kappa_\infty}\frac{\partial G}{\partial y}. \tag{41}$$

Substitution of this definition into the suitably differentiated form of equation (35) yields

$$\nabla^2 W - 3\kappa_\infty^2 W = \left(1 - \frac{1}{\sqrt{3}\kappa_\infty}\frac{\partial}{\partial y}\right)\delta(\boldsymbol{r} - \boldsymbol{r}_0). \tag{42}$$

The function W is now decomposed into two parts as follows:

$$W = W_1 - \frac{1}{\sqrt{3}\kappa_\infty}\frac{\partial W_2}{\partial y}. \tag{43}$$

Then, using the requirement that W_1 and W_2 must vanish for large y, they are both solutions of the equation

$$\nabla^2\begin{pmatrix} W_1 \\ W_2 \end{pmatrix} - 3\kappa_\infty^2\begin{pmatrix} W_1 \\ W_2 \end{pmatrix} = \delta(\boldsymbol{r} - \boldsymbol{r}_0). \tag{44}$$

W was constructed to satisfy the boundary condition $W = 0$ at $y = 0$. This condition is enforced by requiring the following boundary conditions on W_1 and W_2:

$$W_1 = \frac{\partial W_2}{\partial y} = 0. \tag{45}$$

The result of these manipulations is to replace one complex problem for W by two much simpler ones for W_1 and W_2. The solutions for these quantities can be readily expressed in terms of the fundamental Green function shown in equation (28). Denoting this quantity as G_∞ in what follows:

$$W_1 = G_\infty(\boldsymbol{r} - \boldsymbol{r}_0) - G_\infty(\boldsymbol{r} - \boldsymbol{r}_1) \tag{46}$$

$$W_2 = G_\infty(\boldsymbol{r} - \boldsymbol{r}_0) + G_\infty(\boldsymbol{r} - \boldsymbol{r}_1). \tag{47}$$

Here, $\boldsymbol{r}_1$ is the image point of $\boldsymbol{r}_0$ with respect to the $y = 0$ plane, i.e. $\boldsymbol{r}_1 = (x_0, -y_0, z_0)$.

With W known, equation (41) now constitutes an ordinary differential equation for G. Using equations (43), (46) and (47), G can be written in the form

$$G = G_\infty(\boldsymbol{r} - \boldsymbol{r}_0) + G_\infty(\boldsymbol{r} - \boldsymbol{r}_1) + K. \tag{48}$$

The quantity K is the solution vanishing at infinity to the equation

$$K - \frac{1}{\sqrt{3}\kappa_\infty}\frac{\partial K}{\partial y} = -2G_\infty(\boldsymbol{r} - \boldsymbol{r}_1). \tag{49}$$

Introducing the quantities $\lambda = \kappa_\infty\left((x - x_0)^2 + (z - z_0)^2\right)^{1/2}$ and $Y = \kappa_\infty(y + y_0)$, the solution to equation (49) can be readily shown to take the form

$$K = \frac{\sqrt{3}\kappa_\infty}{2\pi}\exp(\sqrt{3}Y)E_1\left[\sqrt{3}\left(Y + \sqrt{Y^2 + \lambda^2}\right)\right]. \tag{50}$$

The Green function is axially symmetric, depending on the three variables λ, $\kappa_\infty y$ and $\kappa_\infty y_0$. Figure 4 shows the integrated intensity distribution associated with a source located at $\kappa_\infty y_0 = 0.3$. The inclination of the contours with respect to the vertical at $y = 0$ determines the heat flux q to the surface. The dependence of this quantity on the distance of the source from the surface is shown in figure 5. The figure shows that as the optical depth $\kappa_\infty y_0$ of

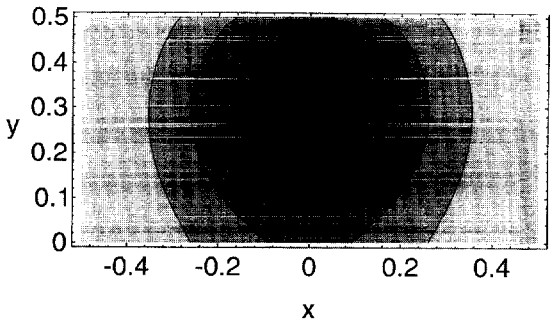

Figure 4. Contour plot of the Green function with a source at $\kappa_\infty y_0 = 0.3$ displayed in units of $1/\kappa_\infty$.

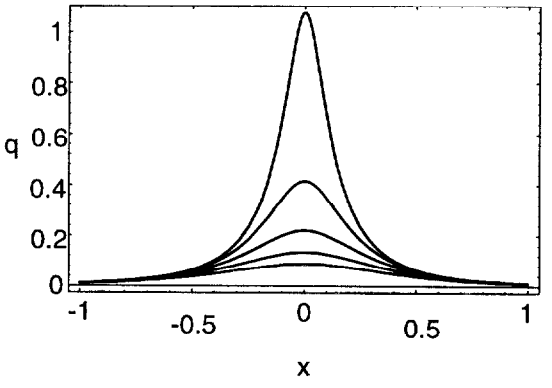

Figure 5. Heat flux to the surface from a point source for source locations $\kappa_\infty y_0 = 0.1$ (top) to $\kappa_\infty y_0 = 0.5$ (bottom).

the source relative to the boundary increases, the flux to the surface decreases rapidly. By the time this quantity reaches a value of one, there is virtually no effect on the surface.

The solution to this radiative transport problem can be regarded as complete once the boundary temperature T_w and the strength of the emitters $\tilde{Q}_n$ are known. The wall temperature is determined in practice by an energy balance in the solid which takes into account heat conduction. The source strength must either be calculated from a local analysis on the scale of the emitting material or specified as a fraction of the chemical heat release which drives the fire. Since the small-scale phenomena which control the chemical heat release are sub-grid scale in the fire simulations for which this model is intended, the details of the local model are not important in the present context. However, it is *very* important to distinguish between radiant energy liberated locally as a result of combustion, and the net energy escaping to remote portions of the spatial domain of interest. The former quantity may be regarded as 'input' into the radiative transport problem, while the latter must be part of the solution.

5. Radiation model in the large-eddy simulation of an isolated fire plume

A typical distribution of thermal elements in a large-eddy simulation (LES) of a square pool fire is shown in figure 6; L_x, L_z and L_y are the physical dimensions of the domain in the two horizontal and vertical directions, respectively. The dark coloured points correspond to thermal elements which locate active combustion and the lighter coloured points are thermal elements for which combustion has ceased. On the base of the domain the radiative

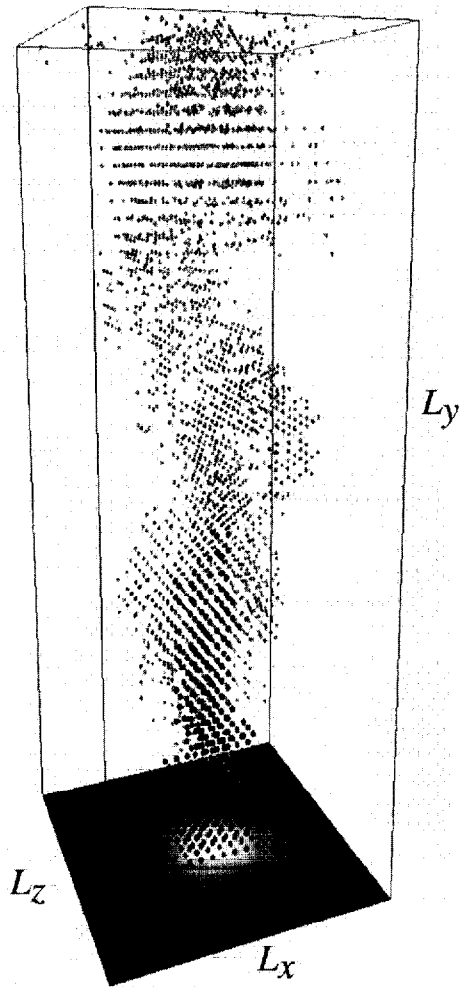

Figure 6. Thermal elements from a large-eddy simulation of a square pool fire. L_x and L_z denote the two horizontal dimensions, and L_y the vertical. Thermal elements which are dark correspond to locations of active combustion, lighter shading denotes elements which have burned out. The radiative flux on the bottom surface is shown by grey-scale contours, lighter shading corresponds to a larger flux.

(This figure can be viewed in colour in the electronic version of the article; see `http://www.iop.org`)

flux on the solid surface is shown by grey-scale contours (lighter shading corresponds to a larger flux). Details regarding the formulation of the LES model are given in Baum *et al* [2, 4]. To date the LES calculations have assumed that a fixed fraction of the chemical heat release is lost by radiation to the surroundings which are radiatively non-participating. Time-averaged LES results and experimental correlations for an isolated fire plume are in good agreement [2]. Indeed, for problems of practical interest a thermal radiation model is the most important improvement to the large-eddy simulation's description of large-scale thermal transport. To this end, the analytical results of section 4 (i.e. equation (39)) were used to test the accuracy of the numerical solution of the P1 approximation for the isolated fire plume case. The solid boundary temperature was assumed to be ambient and the distribution and strengths of the point source emitters were obtained from LES results such as those shown in figure 6.

Within the context of the large-eddy simulation the net volumetric rate of chemical heat release, which appears in the energy equation, is [4]

$$\dot{q}_c(\boldsymbol{r}, t) = \sum_n \dot{Q}_c(t - t_{i,n})\, \delta(\boldsymbol{r} - \boldsymbol{r}_n(t)). \tag{51}$$

Here $\dot{Q}_c$ is the prescribed net volumetric chemical heat release rate of a thermal element; $\boldsymbol{r}_n(t)$ is the position of thermal element n and $t_{i,n}$ is the time at which thermal element n leaves the fuel bed. The value of $\dot{Q}_c$ and its time history are defined such that the fire's total heat release rate and the average flame height are consistent with experimental results. The LES conservation equations for the radiant energy and the integrated intensity are

$$\nabla \cdot \boldsymbol{q}(\boldsymbol{r}, t) = \sum_n \dot{Q}_r(t; n)\, \delta(\boldsymbol{r} - \boldsymbol{r}_n(t)) - \kappa(\boldsymbol{r})\, V(\boldsymbol{r}) \tag{52}$$

and

$$\nabla \cdot \frac{1}{\kappa(\boldsymbol{r})} \nabla V(\boldsymbol{r}) - 3\kappa(\boldsymbol{r})\, V(\boldsymbol{r}) = -3 \sum_n \dot{Q}_r(t, \boldsymbol{r}; n). \tag{53}$$

Here the net volumetric rate of radiant emission for element n is

$$\dot{Q}_r(t, \boldsymbol{r}; n) = \beta \dot{Q}_c(t; n)\, \delta(\boldsymbol{r} - \boldsymbol{r}_n(t)) \tag{54}$$

where β is the prescribed fraction of the chemical heat release rate that is emitted radiatively.

Given the spatial distribution of $\dot{Q}_c$ from the LES calculation, equation (53) was solved with an absorption coefficient which follows a step function in the vertical direction:

$$\kappa(\boldsymbol{r}) = \begin{cases} \kappa_\infty & \text{for} \quad y > 0 \\ \kappa_w & \text{for} \quad y \leqslant 0. \end{cases} \tag{55}$$

A control volume numerical solution approach to equation (53) was used with fast Fourier transforms in the horizontal directions and Gaussian elimination in the vertical direction (direction of variable absorption). The staggered grid used in the LES hydrodynamic calculation was also used in the gas phase part of the radiation calculation. Additional grid points were added to account for absorption in the solid phase. Retaining continuity of both the integrated intensity and the radiative flux across the gas–solid absorption interface was handled in a manner analogous to methods for thermal conductivity interfaces [15].

The following figures show results from a LES simulation of a methanol pool fire. The pool is 30 cm square and the calculational domain comprised of $64 \times 64 \times 128$ cell volumes representing a physical domain of $L_x = L_z = 1.28$ m on the sides and $L_y = 2.56$ m tall. The gas and solid phase absorptions, κ_∞ and κ_w, were defined such that $L_x\kappa_\infty = L_z\kappa_\infty = 4$ and $L_w\kappa_w = 1.25$ (where L_w is the thickness of the solid phase in the radiation calculation).

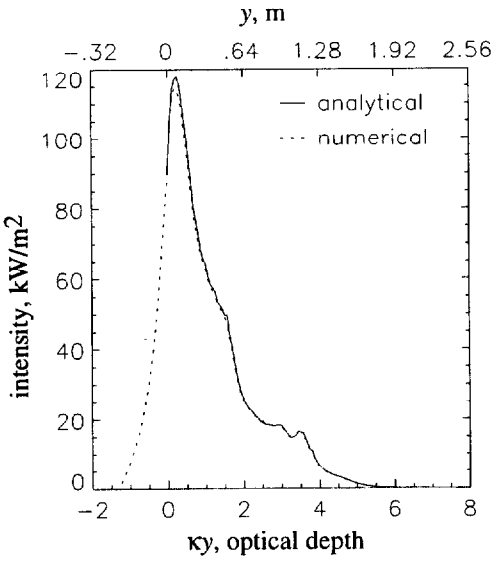

Figure 7. Vertical profile of the integrated intensity, V, above the centre of the pool fire. The intensity from both the numerical (broken curve) and the analytical (full curve) solutions to the radiation transfer equation are shown. Note that the analytical solution is not defined in the solid phase, $\kappa y < 0$.

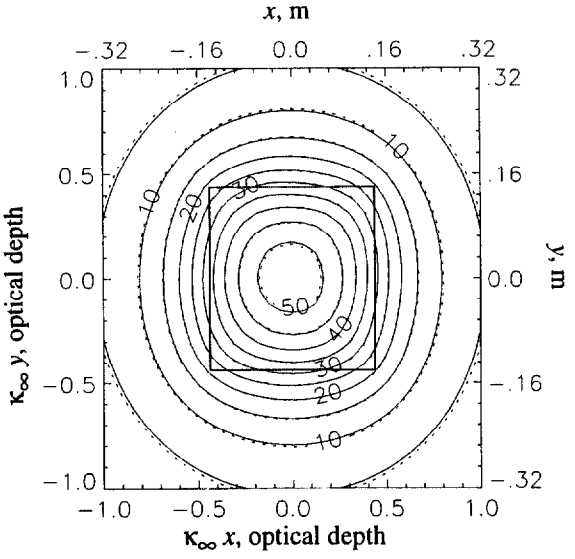

Figure 8. Radiation flux (kW m^{-2}) on the bottom surface. The square outline of the pool fire is also shown. Full curves correspond to the analytical solution and broken to the numerical.

The radiative heat loss fraction was $\beta = 0.2$. Based on experimentally measured mass burning rates the prescribed heat release rate of the pool fire was 260 kW m^{-2}. The active

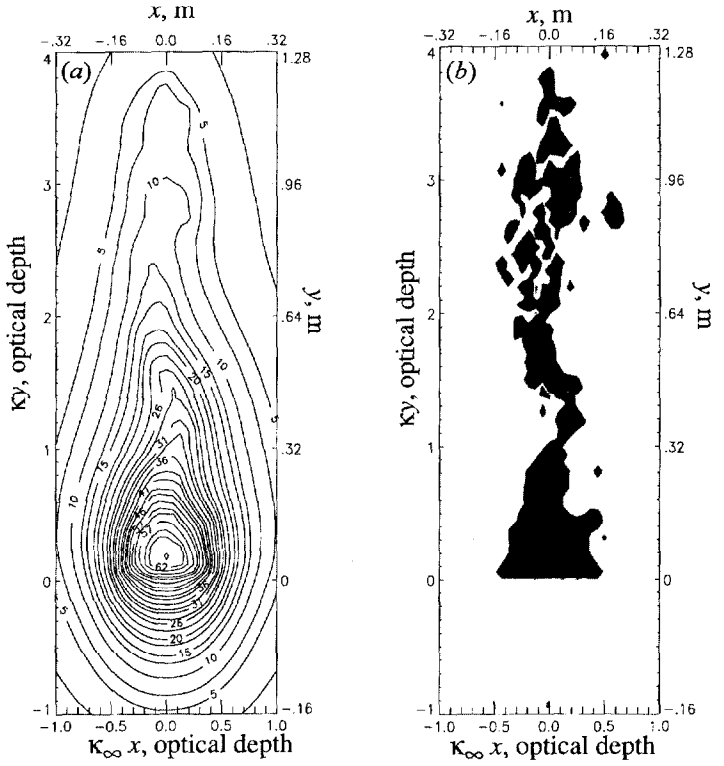

Figure 9. (*a*) Line contours of the integrated intensity (kW m^{-2}) on a vertical plane centred over the pool fire. (*b*) Grey-scale contours of the net volumetric rate of emission in the gas phase. Lighter coloured areas correspond to net emission and darker areas to net absorption.

combustion or flame zone was represented by approximately 36 000 of a total of roughly 80 000 thermal elements.

The numerical calculations were performed on an IBM/RISC 6000 workstation. The computational cost of the large-eddy simulation was 20×10^{-6} CPU s/(cell · timestep); approximately 8 h of CPU time was required for 10 s of simulated real time. Obtaining the integrated intensity from the P1 approximation required 1.3×10^{-6} and 5×10^{-2} CPU s/(cell · timestep) with the FFT-based method and the analytical solution (which used NAG routines to evaluate the exponential integral), respectively. From these timings it is clear that on the scale of the overall LES calculation the P1 approximation is computationally very efficient. Including the P1 approximation in the LES calculation did not require a reduction in the spatial resolution used for the hydrodynamics. Note that this would not have been the case for more expensive models with angular dependence such as the discrete ordinates method.

Figure 7 shows a vertical profile of the integrated intensity above the centre of the pool from both the analytical and numerical solutions of equation (33). The gas–solid interface is at $y = 0$; negative values of the horizontal axis correspond to locations within the solid. The analytical solution (full curve) was determined only for the gas phase. The numerical solution is in excellent agreement with the analytical solution. This agreement allows one to calculate the radiation flux on the surface from the value of the integrated intensity by using equation (34). The radiation flux on the surface is shown in figure 8. Note that the

absorption coefficient of the pool and its surroundings are identical. Again the numerical result is in excellent agreement with the analytical values (full curves). The FFT-based method is clearly an accurate and computationally efficient method for including the P1 approximation in large-eddy simulations of isolated fire plumes with a constant absorption coefficient.

Figure 9(*a*) shows line contours of the integrated intensity on a vertical plane over the centre of the pool fire. In figure 9(*b*) is a grey-scale contour on the same vertical plane of the net volumetric rate of emission; light areas correspond to net emission, dark areas to net absorption. Most emission occurs near the base of the plume. A few areas of high emission exist downstream and originate from thermal elements that rose relatively quickly within the hot core of the plume. Both figures show the presence of fine structures at a resolution which would be prohibitively expensive, computationally, if a radiative transport model with a similar angular resolution were used.

6. Summary and conclusions

The LES technique for simulating fires developed at NIST is based on the assumption that both the chemical heat release and radiative emission occur on subgrid scales. The resources of the computer can then be applied to resolving the buoyancy-generated motion of hot gases and smoke. With present-day computers 3D LES simulations of fire dynamics in which radiative heat transfer is not modelled are possible over scale ranges up to approximately two orders of magnitude. It is highly desirable to incorporate a radiation transport model into the LES approach which is sufficiently efficient that the resolution of the LES is not degraded. By averaging over the angular dependence the P1 approximation is such a computationally efficient radiation model. While other radiation models are available (such as the discrete ordinate method) they are significantly more computationally expensive to use at the desired spatial resolution. Thus, the grey-gas P1 approximation to the radiative transport equation is a suitable radiation model for use in the large-eddy fire simulations.

For the case of a constant absorption coefficient the P1 approximation was found to be in excellent agreement with the exact solution to the radiative transport equation. While the P1 approximation is not limited to constant absorption it is an appropriate first step in the simulation of an isolated fire plume. A fast-Fourier-transform-based numerical solution and the exact solution to the P1 approximation were also compared. The numerical solution was found to be accurate and highly efficient, requiring only a fraction of the total LES computational cost.

For the case of variable absorption coefficients the authors have developed a two-dimensional multigrid numerical procedure for solving the P1 approximation equation. This allows both absorption in depth in solids (e.g. enclosure boundaries) and variable absorption in the gas phase (e.g. soot). This work is currently being extended to three dimensions and will be presented at a later date.

References

[1] De Ris J 1979 *Proc. 17th Int. Symp. on Combustion* (Pittsburgh, PA: Combustion Institute) pp 1003–16
[2] Baum H R, McGrattan K B and Rehm R G 1996 *J. Heat. Trans. Soc. Japan* **35** 45–52
[3] McGrattan K B, Baum H R and Rehm R G 1998 *Fire Safety J.* **30** 161–78
[4] Baum H R, Ezekoye O A, McGrattan K B and Rehm R G 1994 *Theor. Comput. Fluid Dynamics* **6** 125–39
[5] Jia F, Galea E R and Patel M K 1997 *Fire Safety Science, Proc. 5th Int. Symp.* pp 439–50
[6] Lewis M J, Moss M B and Rudini P A 1997 *Fire Safety Science, Proc. 5th Int. Symp.* pp 463–74
[7] Yan Z and Holmstedt G 1997 *Fire Safety Science, Proc. 5th Int. Symp.* pp 345–55

[8] Bressloff N W, Moss J B and Rubini P A 1996 *Proc. 26th Int. Symp. on Combustion* (Pittsburgh, PA: Combustion Institute) pp 2379–86
[9] Bedir H, T'ien J S and Lee H S 1997 *Combust. Theory Modeling* **1** 395–404
[10] Zeldovich Y B and Raizer Y P 1966 *Physics of Shock Waves and High-Temperature Hydrodynamic Phenomena* (New York: Academic) pp 107–75
[11] Siegel R and Howell J R 1992 *Thermal Radiation Heat Transfer* (New York: Hemisphere) pp 771–85
[12] Atreya A and Agrawal S 1998 *Combust. Flame* **115** 372–82
[13] Vincenti W G and Kruger C H 1965 *Introduction to Physical Gas Dynamics* (New York: Wiley) p 495
[14] Pagni P J and Joshi A A 1991 *Fire Safety Science, Proc. 3rd Int. Symp.* (London: Elsevier) pp 791–802
[15] Patankar S V 1996 *Numerical Heat Transfer and Fluid Flow* (New York: Hemisphere) pp 44–7